ACS APPLIED MATERIALS & INTERFACES

Research Article

www.acsami.org

Facile Access to Large-Scale, Self-Assembled, Nacre-Inspired, High-Performance Materials with Tunable Nanoscale Periodicities

Paramita Das,[†] Susanne Schipmann,[‡] Jani-Markus Malho,[§] Baolei Zhu,[†] Uwe Klemradt,[‡] and Andreas Walther*[,†]

[†]DWI at RWTH Aachen University—Interactive Materials Research, Forckenbeckstr. 50, 52056 Aachen, Germany

[‡]II. Institute for Physics B, RWTH Aachen University, 52056 Aachen, Germany

[§]VTT Technical Research Centre of Finland, Tietotie 2, FI-02044, Espoo, Finland

Supporting Information

ABSTRACT: Although advances have been reported to mimic the mechanically excellent structure of natural nacre, larger-scale applications are still limited due to time and energy-intensive preparation pathways. Herein, we demonstrate that simple high-shear homogenization of dispersions containing biobased high molecular weight sodium carboxymethyl cellulose (700 kg/mol, CMC) and natural sodium montmorillonite (MTM), serving as the soft energy-dissipating phase and reinforcing platelets, respectively, can be used to prepare large-area and thick films with well-aligned hard/soft nacre-mimetic mesostructure. During this process, core−shell nanoplatelets with intrinsic hard/soft structure form, which then self-assemble into a layered nanocomposite during water removal. The nanoscale periodicities of the alternating hard/soft layers can be precisely tuned by changing the ratio of CMC to MTM, which allows studying the evolution of mechanical properties as a function of the lamellar nanoscale periodicity and fractions of hard to soft material. Remarkable mechanical stiffness (25 GPa) and strength (320 MPa) can be obtained placing these materials among the top end of nacre-inspired materials reported so far. Mechanical homogenization also allows direct preparation of concentrated, yet homogeneous, gel-like dispersions of high nanoclay content, suited to doctor-blade large-area and thick films with essentially the same properties as films cast from dilute dispersions. In terms of functional properties, we report high-transparency, shape-persistent fire-blocking and the ability to surface-pattern via inkjet printing. Considering the simple, fully scalable, waterborne preparation pathway, and the use of nature-based components, we foresee applications as ecofriendly, bioinspired materials to promote sustainable engineering materials and novel types of functional barrier coatings and substrates.

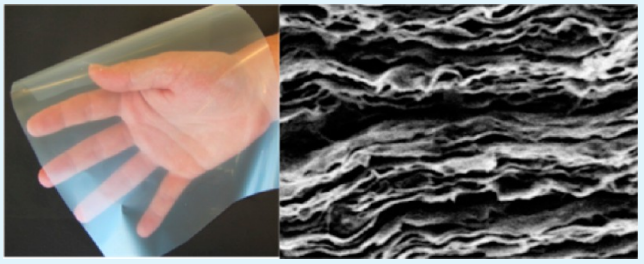

KEYWORDS: *biomimetic materials, layered nanocomposite, structure−property relationships, self-assembly, nacre*

INTRODUCTION

Nature's load-bearing materials are paradigms for lightweight engineering as they uniquely combine stiffness, strength, and toughness with low density.[1,2] Spider silk, wood, mother of pearl (nacre), crustacean cuticles, and bone are some prime examples. Such biocomposites are characterized by ordered structures combining large fractions of hard, reinforcing segments with a minor amount of soft, energy-adsorbing, lubricating biopolymer. The interface between hard and soft is durable and well-controlled. Nacre exhibits a brick-and-mortar architecture in which 95 vol % of $CaCO_3$ microtablets are arranged in a minority phase of biopolymer. Due to its extraordinary mechanical properties, nacre has inspired the fabrication of bioinspired, layered nanocomposite materials.[3−5]

Some of the main lessons for nacre-inspired composites are the layered, highly oriented arrangement of the reinforcements, the alternating hard and soft layers, tailored interactions of the soft phase and the presence of a majority fraction of reinforcements. These aspects also fundamentally distinguish bioinspired nanocomposites from traditional ones, which only use low contents of reinforcements (<10 wt % nanoclay). Seashells are able to grow these complex materials in water in a lengthy process.[6] However, for man-made structural materials manufacturing such slow growth strategies are not applicable and new time-efficient self-assembly strategies are needed to prepare similarly structured material. Finding access routes to such large-scale complex materials with high fractions of reinforcements and easily tunable nanoscale structures still remains a considerable scientific challenge.

Strategies for nacre-inspired materials often use sequential deposition strategies, such as layer-by-layer (LbL) deposition of nanoclays and polymers or alternating spin-coating of thin polymer layers and monolayer deposition of platelets.[7−13] These approaches led to remarkable properties, where for

Received: January 26, 2013
Accepted: March 28, 2013
Published: March 28, 2013

example high stiffness and strength, or good stiffness and high ductility, were achieved. Although demonstrating interesting property profiles, these materials are tedious to prepare and restricted to finite dimensions with very small thickness. Other approaches to layered composite materials deal with ceramic-type of processing using ice-templating, sintering, and infiltration of resins, deposition of platelets in electric fields, or controlled sequential crystal growth of $CaCO_3$ in a layered fashion.[14−20] Frequently, only structural control is demonstrated and mechanical or functional properties are not described, which in some cases relates to the too small material dimensions.

A simpler access route could be provided by direct cocasting of polymers and nanoclay, which can give rise to self-assembling lamellar films during water evaporation.[16,21−26] For such an approach, stable dispersions without coagulation and phase separation at high nanoclay contents are crucial and require the control of interactions. In fact, much attention in concentrated polymer/clay systems was drawn to understanding the dispersion characteristics and structure formation processes.[16,21,23,26−34] However, comparably little effort was directed to using such self-ordering structures to realize mechanically excellent high-performance bulk materials and to use the capabilities for a dedicated tuning of the nanostructures across the full composition range and up to high clay contents.[21,23,27] One of the most notable co-casting approaches at high clay loadings was reported by Ebina et al. describing transparent, layered nanoclay/polymer films, which showed high thermal resistance and good gas barrier properties in the presence of only 10 or 20 wt % of water-soluble polymer binder. Due to the small lateral size of the nanoclay, the binder mostly localized at the cationic rims of the nanoplatelets. Although displaying attractive functionality, the material only had very low tensile strength around 25 MPa at strain to failure of 1.8%, thus falling short of nacre-mimetics targeting the highest mechanical properties. Shikanaka et al. reported related transparent lamellar PEO/laponite films with 57 wt % nanoclay, yet also with low stiffness and strength of 11 and 28.7 MPa, respectively, at low elongation.[35−37] In the case of larger montmorillonite, Zhu et al. investigated the effect of salts on the structure and properties of layered PVA/MTM materials and discussed mechanical properties at 55 wt % nanoclay, yielding Young's modulus and tensile strength between 6 and 11.5 GPa and 20−45 MPa, respectively, at elongations of 4−22%.[38] Consequently, although there has been progress, success toward very strong and stiff nacre-inspired materials based on such a simple approach using widely available materials is limited and crucial advances need to be made.

We recently developed a water-based approach that allowed self-assemblies into nacre-inspired materials based on highly purified polymer-coated core−shell nanoclays.[39,40] These core−shell platelets were prepared via adsorption of a single polymer layer on top of montmorillonite (MTM) nanoclays, by slow addition of a dilute nanoclay dispersion to excess synthetic polymer (e.g., polyvinylalcohol) and subsequent separation of excess polymer via centrifugation/redispersion cycles to maximize the fraction of reinforcements in the final material. Excess polymer was crucial to prevent coagulation due to the strong interactions of both components. After film formation, this has enabled high modulus (27 GPa) and high strength (165 MPa) at a majority fraction of 70 wt % reinforcements combined with low density and we could demonstrate covalent and supramolecular cross-linking to increase the properties. A similar approach was later on presented by Yao et al. for chitosan/MTM self-assemblies.[41]

Although thick films could be prepared, this dedicated self-assembly approach suffers from a crucial bottleneck, that is the need for an intermediate extensive purification step via centrifugation/redispersion cycles to isolate pure core/shell building blocks. Therefore, we were asking the question whether this purification step can be overcome by directly using optimized dispersions of nanoclay and polymer, and subsequent direct self-assembly into nacre-inspired films. The principal feasibility of such a strategy is indicated by the ability of nanoclay/polymer mixtures to form defined lamellar phases and well-ordered films (see discussion above, e.g. PEO/laponite), given the interactions are properly mediated and coagulation is prevented.

In addition, most of the present nacre-mimetic materials are based on polymers from petrochemical origin. In the light of finding sustainable alternatives for future materials, we also turned our attention to renewable polymers—with cellulose being the major relevant polymer due to its large-scale and global availability.

Herein, we will show how homogeneous dispersions of anionic sodium carboxymethylcellulose (CMC) and anionic montmorillonite (MTM) can be used to fabricate highly oriented, layered, thick, large-area nanocomposites with remarkable mechanical properties. Stiffness (25 GPa) and strength (320 MPa) are among and partly above the best ever reported properties for nacre-inspired materials. We will derive the influence of the nanoscale thickness of the soft, energy-dissipating, organic layer on the macroscopic mechanical properties by varying the nanoscale periodicity of the alternating hard/soft layers via adjusting the feed composition. Furthermore, we demonstrate that nanostructural control can also be maintained when the materials are adequately mixed in highly concentrated suspensions to allow for slurries that are directly suitable for doctor-blading into large-area films. In addition to excellent mechanical performance and direct material preparation from concentrated dispersions, we show functional benefits, such as transparency, the possibility to print on these materials, and fire-blocking.

EXPERIMENTAL SECTION

Materials. Sodium carboxymethyl cellulose (CMC, degree of substitution = carboxymethyl groups per anhydroglucose unit = 0.9; M_w = 700 kg/mol, Aldrich), Na-Cloisite (montmorillonite, MTM, Rockwood), and Milli-Q water were used for all experiments.

Preparation of Nacre-Inspired Films. *Films Cast at High Dilution.* MTM was dispersed as a 0.5 wt % dispersion overnight and subsequently slowly added to a Philips HR2094/00 blender (750 W) containing a strongly agitated 0.25 wt % solution of CMC until the desired weight ratio was obtained. Thereafter the dispersions were homogenized for a further 5 min, degassed to minimize voids in the final materials, poured into Petri dishes to cast films, and dried at ambient conditions. Accelerated drying can be performed at 50 °C providing fully dried films within a day, depending on the thickness.

Doctor-Bladed Films from High Solid Dispersions. MTM was slowly added as powder to an IKA HKD-T-0.6 high-performance kneader with two wide-bladed kneading elements, containing a 2.5 wt % CMC solution until the desired CMC/MTM ratios were obtained. After homogenization for 12 h and degassing within the kneader, the soft gels were doctor-bladed onto PET foils and dried at ambient conditions within 1 day. Accelerated drying can be performed at 50 °C providing fully dried films within a few hours, depending on the thickness.

Scheme 1. General Strategy to Self-Assembled, Nacre-Inspired Films Based on Renewable Sodium Carboxymethyl Cellulose (CMC, R = H or CH_2−COONa) and Naturally Sourced Montmorillonite (MTM)[a]

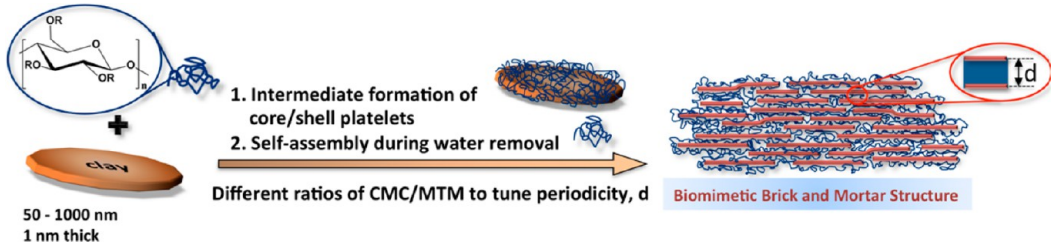

[a]Core−shell platelets are formed at an intermediate state due to polymer adsorption on the nanoclay surface. The nanoscale periodicity, *d*, of the nacre-mimetics can be tuned by adding additional free polymer in the feed.

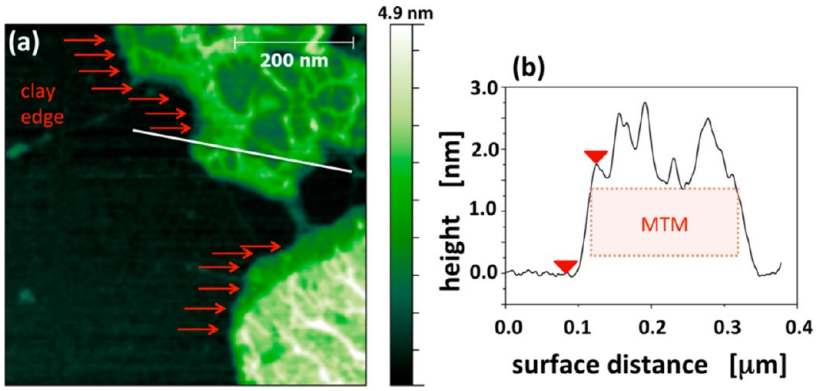

Figure 1. (a) Atomic force microscopy image obtained after centrifugation and redispersion (to remove excess polymer) of a dispersion of CMC/MTM = 60/40. Two hard/soft core−shell nanoplatelets are depicted on the right-hand side. A thin polymer coating can be identified on (and underneath) the MTM nanoclays. The sample was deposited onto mica. (b) Height profile of the white line in part a.

Inkjet Printing. Inkjet printing was performed using standard printer settings and commercial Canon inks on a Canon Pixma iP4950 inkjet printer.

Analysis. Scanning electron microscopy (SEM) was performed on a Hitachi S-4800 field emission microscope (1.5 kV) after sputter-coating a thin gold layer.

Thermogravimetric analysis (TGA) was done using a NETZSCH TG 209C instrument under continuous flow of 25 mL/min of N_2 at a heating rate of 20 K/min.

Scanning force microscopy (SFM) was performed on a Veeco Multimode in tapping mode conditions using standard silicon cantilevers (PPP-SEIH-W from Nanosensors).

Transmission electron microscopy (TEM) was performed on a JEOL JEM-3200FSC Cryo-TEM, operating at liquid nitrogen temperature. Zero-loss filtered images were obtained at an acceleration voltage of 300 kV. All images were registered digitally by a bottom mounted CCD camera system (Ultrascan 4000, Gatan) combined and processed with a digital imaging processing system (Gatan Digital Micrograph 3.9 for GMS 1.4). Microtomed ultrathin sections were obtained using a LEICA 125 Ultracut microtome. The samples were embedded into epoxy resin prior cutting.

Wide-angle X-ray scattering was performed at the small- and wide-angle X-ray scattering beamline MiNaXS beamline P03 at HASYLAB Hamburg, Germany. Scattering data was recorded using a 13 keV (0.954 Å) X-ray beam with a beam size of 22.0 μm × 17.1 μm and a Pilatus 300k detector at a sample to detector distance of 421 mm.

Mechanical tests were carried out on a DEBEN minitester equipped with a 20N load cell. All measurements were conducted at room temperature and an average humidity of 23%. The specimen sizes used were typically in the range of 2 cm × 2.25 mm × 30−50 μm. At least five (mostly eight) specimens were tested for each sample. A nominal strain rate of 1 mm/min was used. The slope of the linear elastic region of the stress−strain curves was used to determine the Young's modulus, *E*.

RESULTS AND DISCUSSION

The herein used concept toward facile, large-scale, nacre-inspired films based on natural building blocks is summarized in Scheme 1. First CMC/MTM hydrocolloid dispersions are prepared by high-shear mixing at different weight ratios with a focus on high ratios of nanoclay up to 90 wt %, followed by film casting. During film casting self-assembly into lamellar dispersion phases takes place, which upon drying leads to highly ordered bulk films. The stacking distance of the nanoclays in the final material, *d*, is controlled, as will be shown below, by the feed ratio of the components as additional free polymer will contribute to an expansion of the organic phase.

One of the most important prerequisites to allow for the formation of ordered bioinspired polymer/nanoclay hybrid films from water is to prevent premature aggregation and coagulation of the components in the aqueous phase, which is especially problematic at low polymer content favoring bridging of nanoclays. Therefore, we chose anionic CMC to prevent flocculation in the presence of anionic MTM, as opposed to, e.g., using strongly electrostatically interacting cationic polysaccharides such as chitosan. Some interaction was yet expected as MTMs have a cationically charged rim able to bind anionic CMC and because there is an entropic driving force to adsorb hydrophilic, only slightly charged polymers onto the basal planes of nanoclays.[42] During water removal, additionally present hydrogen bonds between MTM and CMC can strengthen further and form a strong interfacial attachment needed for stress transfer.[43,44]

Aside from designing the system chemically, attention needs to be drawn to optimize physical mixing and addition protocols. We used a very high molecular weight CMC (700 kg/mol) to target the best mechanical properties, yet this adds a challenge as it leads to very viscous solutions already at high dilution (ca. 4000 mPa·s at 1 wt %). Therefore, to prepare most homogeneous dispersions, we slowly added a previously well-homogenized 0.5 wt % dispersion of MTM (Na^+Cloisite) to a 0.25 wt % dispersion of Na^+CMC (700 kg/mol, 0.9 carboxymethyl groups per anhydroglucose unit) in a high shear mechanical blender until the desired ratio of organic to inorganic material was obtained. This method provides substantially higher shear than in standard lab equipment (magnetic stirrer). Note that MTM is already majorly exfoliated into single ca. 1 nm thick nanoplatelets in the utilized 0.5 wt % dispersion in water. The ratios were selected in a wide range of CMC/MTM (9/1, 8/2, 6/4, 4/6, 2/8, 1/9 w/w) to monitor the full behavior of the system. Importantly, the addition of nanoclay to polymer minimizes potential bridging of several nanoclay particles by single polymer molecules, which can be observed as flocculation when small amounts of binding polymers are added to a nanoclay dispersion. In combination with the high shear mixing, all CMC/MTM dispersions were homogeneous to the naked eye, indicating efficient dispersion of both components.

To experimentally access the solution state, we conducted atomic force microscopy (AFM) investigations of dispersions containing CMC and MTM. Figure 1 displays an AFM image obtained after one centrifugation and redispersion cycle to remove excess polymer, which would hinder clear imaging.

Figure 1 shows two flat and large nanoclay sheets, several hundred nanometers in diameter, that are partly coated by a thin layer of CMC. The CMC coating is evident due to the increased height (see section analysis) and the rough surface on top of the nanoclay. Pristine nanoclay shows an extremely flat surface and an average height close to 1 nm.[39] Note that the substrate surface is clean of polymer, and thus, the coating does not arise during drying of a solution. The driving force for binding on the basal surface is three-fold. Elemental analysis of the MTM revealed the presence of Ca^{2+} counterions within the Na^+MTM (0.45 wt % of total MTM content). Due to their mutlivalency, they remain more tightly condensed to the highly charged MTM surfaces as compared to monovalent Na^+ counterions.[45−48] Thus, the carboxylate groups of CMC can bind to them in addition to hydrogen bonding between alcohol and acid groups of the CMC and Si−O−Si units on the nanoclay surface, and the known entropic adsorption of polymers on the basal nanoclay planes.[42−44] AFM thus confirms that well-defined core−shell platelets are intermediately formed during the mixing, allowing for an efficient stress transfer in bulk. Their encoded order is transferred into layered hybrid films. Importantly, the stacking distances can be controlled by additional polymer in solution, as will be shown in wide-angle X-ray scattering below (Figure 3, Table 1).

The layered bulk nanocomposites were prepared by simple film casting of the various CMC/MTM dispersions. During the evaporation of the water, the concentration of the core−shell nanoclay platelets increases and they start to organize in a layered/lamellar structure due to hydrodynamic interactions. This process allows large-area and also thick films, typically prepared with thicknesses in the range of 30−200 μm. Accelerated drying at 50 °C can provide films within 1 day. Faster time scales may be achieved by increasing the temperature or concentration (see below) but are not in the main scope of this contribution.

Table 1. Structural and Mechanical Properties of Nacre-Inspired CMC/MTM Films

CMC/MTM	nanoclay content [%][a]	spacing MTM [nm][b]	E [GPa]	σ_{UTS} [MPa]	ε_{max} [%]
90/10	nd		14.1 ± 1.2	259 ± 9	5.6 ± 0.4
80/20	19.1		21.5 ± 2.5	319 ± 12	2.6 ± 0.2
60/40	40.5	2.71	24.6 ± 1.9	251 ± 20	1.5 ± 0.2
40/60	63.4	1.90	20.1 ± 3.9	217 ± 17	1.3 ± 0.6
20/80	83.4	1.43	16.6 ± 3.6	142 ± 10	1.0 ± 0.1
10/90	90.8	1.34	6.8 ± 2.0	74 ± 5	1.5 ± 0.3

[a]Determined by TGA in the plateau area from 550 to 600 °C. nd = not determined. [b]Determined by WAXS. The basal spacing of pure MTM was determined to be 1.2 nm corresponding to the hydrated structure.

Figure 2 displays scanning and transmission electron microscopy (SEM and TEM) images of the resulting nanocomposites at different weight fractions (see also Figure S1 of the Supporting Information). The SEM images clearly show the desired layered arrangement over large areas, independent of the ratio of CMC/MTM used. Due to the large size of the nanoclays, tight interlocking can be formed by nanoclays branching from one layer into other ones (Scheme 1). We further recorded TEM images of a microtomed, ultrathin cross section of a selected nanocomposite to support the alternating hard/soft layers. Figure 2d depicts the TEM image of CMC/MTM = 20/80, in which well-spaced alternating dark (nanoclay) and gray (polymer) layers can be identified, as also further highlighted by a greyscale section analysis. The spacing is roughly 1.65 nm, which is larger compared to pristine MTM and indicates a thin polymer layer in between. Due to distortions during microtoming of these stiff materials, the distances need to be treated with some care.

Hence, to achieve a more quantitative understanding of the periodicities, we further performed wide-angle X-ray scattering (WAXS) at different beam inclinations with respect to the observed orientation of the nanoclay layers using a high intensity synchrotron X-ray source. All WAXS curves were measured with the same time and intensity to allow for comparison.

The 2D detector images demonstrate the absence of scattering events for an X-ray beam irradiating perpendicular to the plane (Figure 3b) and in 40° (not shown). Diffraction peaks start to appear upon irradiation at shallow angles, here displayed for ca. 15° (Figure 3c). Most importantly, the diffraction peaks are strongly confined within two opposing arcs of small azimuthal width. Both effects confirm highly ordered systems. Integrations along the scattering vector in a window of ±20° centered on the Bragg peak allow the quantification of the gallery spacing between the nanoclays (see Figure 3a). The scattering curves show a distinct shift of the primary scattering peak from the known distance of pure MTM in hydrated conditions (1.2 nm) to smaller q-values with increasing content of polymer (see Table 1). This confirms the successful intercalation of the MTM galleries during the restacking in the drying procedure. The distance between the nanoclays consistently increases with rising polymer content (see inset Figure 3a), demonstrating the desired control of the nanostructure of the materials.

dx.doi.org/10.1021/am400350q | ACS Appl. Mater. Interfaces 2013, 5, 3738−3747

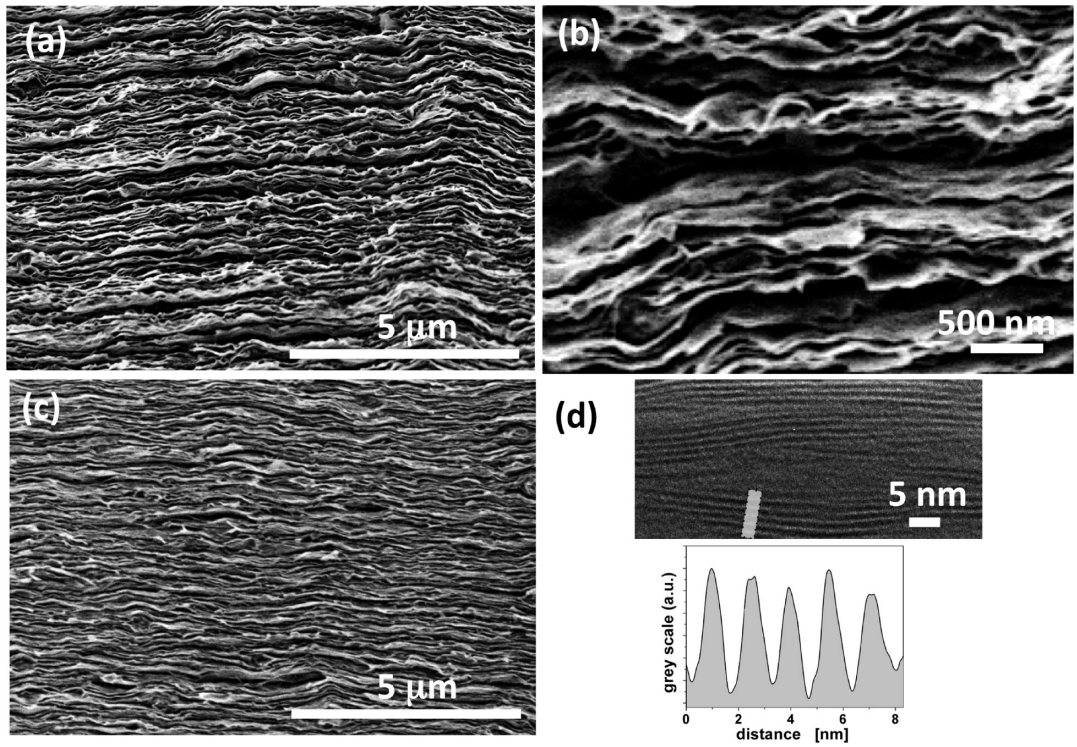

Figure 2. Electron microscopy characterization: (a and b) SEM images of layered nanocomposites at CMC/MTM = 20/80 and (c) CMC/MTM = 40/60. (d) TEM image of an ultrathin cross section of CMC/MTM = 20/80 with a cross section analysis highlighting the alternating hard and soft layers. Further SEM images of other compositions can be found in Figure S1 in the Supporting Information.

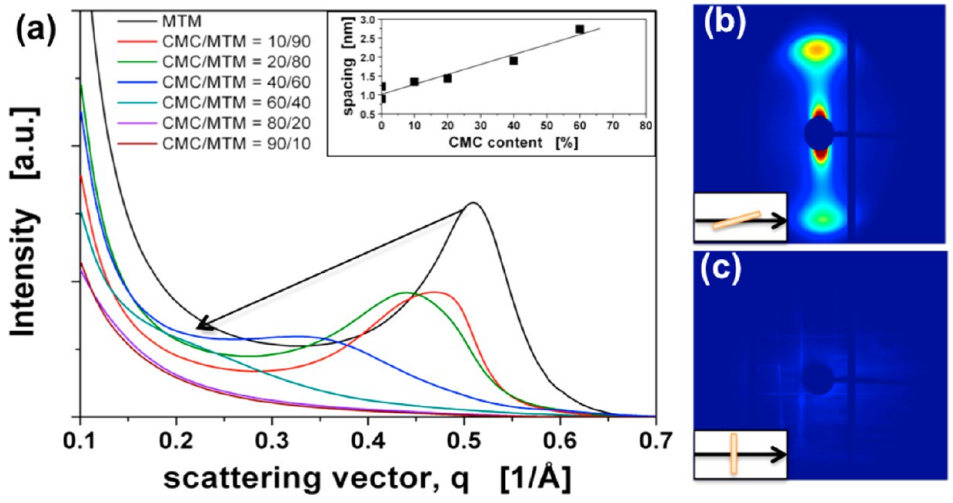

Figure 3. (a) Wide-angle X-ray scattering curves obtained for various composites and measured with the same intensity and time. (inset) Spacing calculated from the primary scattering peak (q^*) according to $2\pi/q^*$ as a function of the content of CMC. Both dehydrated (0.9 nm) and hydrated (1.2 nm) basal spacings of MTM are shown. The line serves to guide the eye. (b and c) Exemplary 2D scattering images obtained for CMC/MTM = 20/80 at different beam inclinations with respect to the plane of the film [(b) 15° and (c) 90°] as schematically shown in the bottom left corners.

We emphasize that the system is near quantitatively exfoliated in solution and restacked in bulk, as a scattering peak for completely non-intercalated MTM can hardly be observed. Nonetheless, the only small increase of the gallery spacing at 10 wt % of CMC indicates that the polymer is not present as a continuous layer, but that MTM faces touch at certain points. From earlier investigations on the self-assembly of purified core−shell polymer-coated nanoclays, effectively covered with exactly one monolayer of polymer on each nanoclay, we know that the final materials contain roughly 20−30 wt % polymer and exhibit continuous polymer layers in-between the nanoclay stacks.[39,40] In these systems, in fact a polymer double layer is formed in-between the stacks during the assembly of two polymer-coated nanoclays on top of each other. Consequently a continuous polymer layer can already be formed at slightly lower weight fractions, depending on the type of polymer used. Earlier investigations by Ebina et al. discussed adsorption of an anionic polymer in polyanion/nanoclay at the cationic rims of much smaller nanoclay, Na^+saponite, with lateral dimension much smaller than 50 nm.[17,18] In such systems using ultrasmall nanoclays, edge effects are dominant,

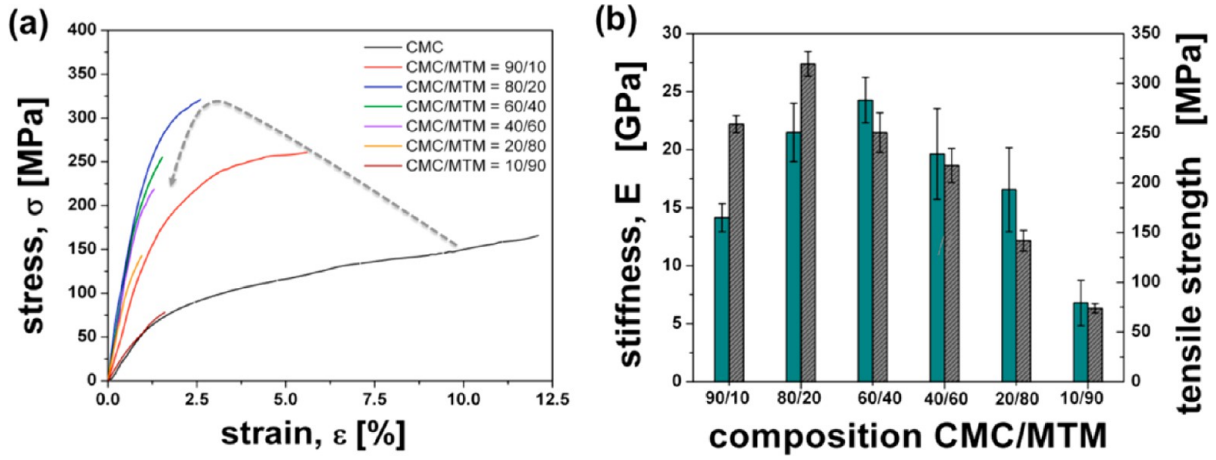

Figure 4. (a) Mechanical tensile tests of CMC/MTM films of various compositions as indicated within the figure. The arrow serves to guide the eye from low to high fractions of MTM. (b) Stiffness (cyan, left column) and tensile strength (gray, right column) as a function of the composition.

whereas this is not the case for the much larger MTM employed herein.

It can further be observed that the peak intensity diminishes for increasing polymer fractions, which originates from a wider distribution of stacking distances and loss of long-range correlation to allow for appearance of a Bragg peak. Large polymer contents above 60 wt % do not allow to identify any distinct stacking distance anymore, but the layered structure is unambiguously confirmed by SEM imaging (Figure 2 and Supporting Information Figure S1).

Consequently, both imaging and scattering data confirm that well-defined, highly ordered, near quantitatively exfoliated and restacked bionanocomposites can be obtained with this simple, high-shear blending approach. Unwanted flocculation and ill-defined structure formation are absent due to the choice of polymer, addition sequence, and high shear homogenization protocol. The nanoscale stacking periodicity is controlled by the amount of polymer within the nanoclay dispersion and allows tailoring the gallery spacing in the restacked, nacre-inspired films with high structural control. The mesostructures closely resemble the ones found in previous and more time-consuming nacre-mimetics based on LbL or self-assembly of purified core−shell nanoplatelets.[7−9,39−41] However, the precise tuning of the gallery spacing is a distinct advantage of this procedure and allows us to look in detail how mechanical properties change as a function of the hard/soft ratio from moderate to very high nanoclay content. The corresponding mechanical tensile testing data are summarized in Figure 4 and Table 1.

Pure high molecular weight CMC (700 kg/mol) already displays good tensile properties (Young's modulus E = 5.8 GPa, tensile strength σ_{UTS} = 151 MPa, elongation at break ε_{max} = 12.1%). These values are better in terms of stiffness, strength, and also in elongation at break, as compared to CMCs of lower molecular weight, which are easier to use in bulk material applications due to simpler handling in solution. Nonetheless, using this very high molecular weight CMC, although being more difficult to apply due to high viscosities, contributes to the overall good mechanical performance.

Starting from pure CMC, it is obvious that continuous addition of nanoclay leads to a stiffening and strengthening of the material up to a weight ratio of ca. 20−40 wt % (Figure 4b), originating from an efficient stress transfer from the CMC matrix to the MTM reinforcements. Upon reaching 40 wt % of nanoclay and further addition, a decrease of the tensile strength and for even larger fractions also a decrease of stiffness can be observed. Lower tensile strength can be explained by the increasing brittleness of the materials, which leads to early fracture based on cracks propagating from surface defects. Additionally, the WAXS measurements showed that the average stacking distances between the nanoclays becomes so small for low fractions of polymer (10 wt % CMC), that it is physically impossible for the nanoclays to have a fully continuous soft polymer layer in between them throughout the full nanoclay interfaces. Therefore, some parts of the MTM platelets should be in direct contact and do not have any possibility to dissipate stress and fracture energy in a soft polymer phase intercalated between them. Incomplete activation of the nanoclay surface by CMC explains the observed lower stiffness at clay fractions larger than 80%.

Overall, we find an interesting optimum performance at 20−40 wt % of MTM considering the need to balance highest mechanical properties (Figure 4b) and functional properties for instance in fire and gas barrier materials that benefit from large fractions of exfoliated nanoclay. Larger amounts of nanoclay may still be interesting for barrier applications, but in terms of mechanical properties, fractions of MTM ≥ 60% correspond to an overloading in this material combination. All values are summarized in Table 1. Already at this point, it is important to emphasize that we achieve remarkable mechanical properties, combining high tensile strength, σ_{UTS}, close to 320 MPa with high stiffness (Young's modulus, E) up to 21.5 GPa for CMC/MTM = 80/20. Importantly, we also still find 2.5% maximum strain, which is significantly above typical nacre-mimetics that break at strain close to or below 1%.[7−9,39−41] The additional strain provides means for efficient fracture energy dissipation due to frictional platelet sliding.

Next, we compare the mechanical properties to earlier nacre-inspired materials based on polymer/nanoclay composites. Since lightweight character is one of the profound motivations to pursue biomimetic material concepts, we also report the specific material properties in a materials selector chart as introduced by Ashby and Wegst (Figure 5).[49] In the field of polymer/nanoclay-based, nacre-inspired materials Kotov et al. reported a range of systems prepared by LbL, also including post and sequential cross-linking procedures.[7−9] Notably the best system was produced by stepwise LbL deposition of PVA and MTM and intermediate cross-linking using glutaraldehyde,

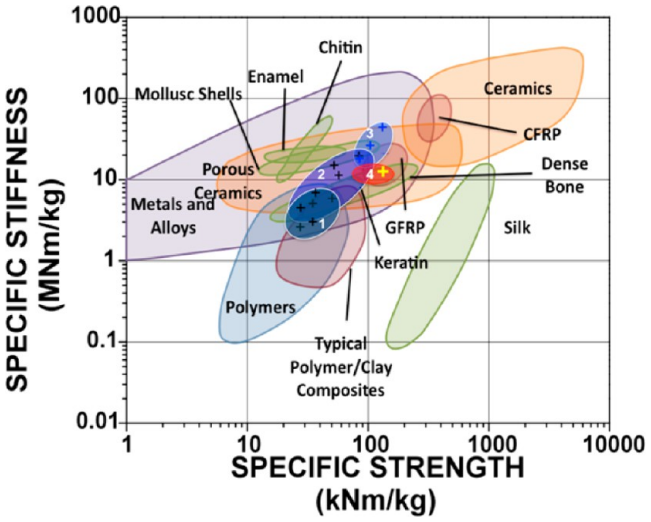

Figure 5. Specific materials selector chart[49] concerning lightweight engineering materials, highlighting different materials classes. The best materials are top-right in this plot. Nacre-inspired polymer/nanoclay materials are shown according to their preparation pathways: (1 cyan) non-cross-linked LbL materials;[8,9] (2 dark blue) dedicated self-assembly approach using purified core–shell nanoclays;[39−41] (3 light blue) cross-linked LbL materials;[7,8] (4 red) materials of the present study with the yellow mark denoting CMC/MTM = 80/20. The mechanical performance of classical polymer/nanoclay composites is estimated based on a recent review.[27] Densities of the material were estimated based on the known values for the components and the reported fractions of inorganic materials.

leading to stiff and strong nanocomposites at ca. 70 wt % of inorganic (light blue region).[7] In general, the properties for very thin LbL films with ca. 70 wt % of nanoclay span a wide range. Non-cross-linked materials are typically in a range of Young's modulus = 6−15 GPa and ultimate tensile strength of 75−150 MPa (cyan region 3).[8,9] Ionic cross-linking can be used to increase these properties to roughly double or triple these values (light blue region 1).[8] The dark blue region (2) displays the area corresponding to the materials prepared by dedicated self-assembly of purified core−shell nanoclays. The best material is found at the top right and was prepared by post-cross-linking of PVA/MTM films with borates. We also include the best values so far reported for bionanocomposites with layered architectures, i.e. nanoclay/chitosan prepared via either LbL[9] or using the dedicated self-assembly of core/shell colloids[41] (Young's modulus = 6−10 GPa and ultimate tensile strength 75−100 MPa).

With respect to previous co-cast films, we also again refer to earlier work by Ebina, who used a small Na^+saponite nanoclay (diameter < 50 nm) bound with small amounts of anionic polyelectrolytes including CMC. Despite demonstrating excellent gas barrier properties, the materials show brittle behavior and less than one tenth of the tensile strength achieved here (Na^+saponite/poly(sodium acrylic acid) = 90/10 w/w: σ_{UTS} = 25 MPa, ε_{max} = 1.8%, Young's modulus not reported).[18,50] This is clearly due to using excess reinforcements, as also confirmed in our studies when approaching such extreme nanoclay contents (Figure 3). Further relevant previous co-cast polymer/nanoclay materials to compare to are (i) PEO/laponite (57 wt % laponite, laponite diameter < 30 nm; E = 11 MPa and σ_{UTS} = 28.7 MPa) and (ii) PVA/MTM (55 wt % MTM; E = 6−11.5 GPa and σ_{UTS} = 20−45 MPa).[36,38] From this comparison, it becomes evident that our purposefully designed system exceeds previous co-cast self-assembling polymer/clay films considerably, partly by 1 order of magnitude.

Moreover, also with respect to nacre-mimetic materials,[7−9,39−41] we report excellent and highly competitive properties (Young's modulus up to 21.5 GPa and a tensile strength close to 320 MPa). This excellent performance can also be seen by adding them to the Ashby plot in Figure 5 (red region 4), notwithstanding the fact that Na^+CMC itself has a comparably high density of 1.6 g/cm^3 in relation to other polymers. Although they cannot yet reach the specific stiffness of the ultrastiff and strong, cross-linked, sequentially prepared (PVA/MTM) LbL materials,[7] they exceed them already in terms of specific strength and occupy a previously unachieved property area. In fact, to the best of our knowledge the tensile strength is the highest ever reported one for non-cross-linked nacre-inspired materials and exceeds natural nacre considerably (tensile strength = 60−140 MPa).[1,2] It is also important to note that the best CMC/MTM materials surpass the values for other biobased nacre-mimetics using chitosan up to three times in terms of stiffness and strength, at comparable elongation at break.[9,41] Hence the present materials are also significantly tougher, considering the integral area under the stress/strain curves as an estimate for the work-of-fracture. We foresee that cross-linking procedures are able to further augment the present properties as it was seen for LbL based materials and the dedicated self-assembly approach using purified core/shell

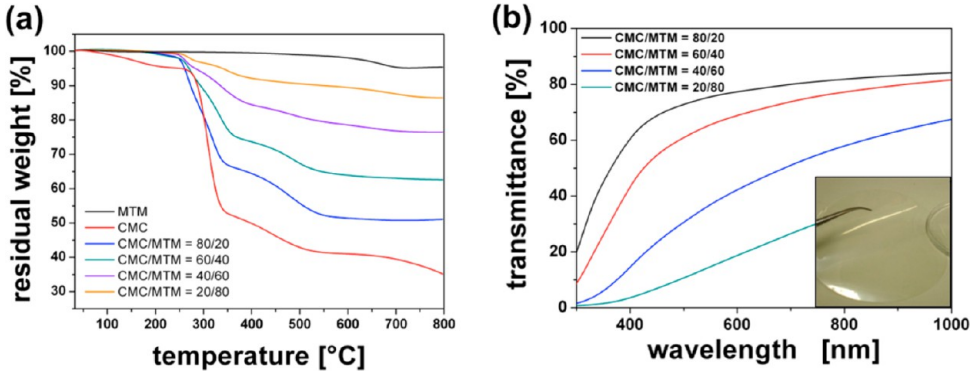

Figure 6. (a) Thermal degradation profiles measured by thermogravimetric analysis of various nanocomposites and the two starting materials. (b) UV−vis transmittance of various composite films at a thickness of 40−50 μm. The inset depicts a flexible and transparent foil of the composition CMC/MTM = 60/40.

platelets. Overall, the present performance area places these nacre-inspired bionanocomposites in competition with glass fiber reinforced plastics and selected metals. They exceed classical polymer/nanoclay nanocomposites[27] by 1 order of magnitude.

From a fundamental viewpoint, it is important to realize that the nanoclay loadings in any of the previous sophisticated approaches to nacre-mimetics using LbL or self-assembly of purified core/shell platelets (MTM ≥ 70 wt %)[7−9,39−41] might in fact be too high to obtain sufficient dissipation of fracture energy in the soft phase to allow for some shear deformation between the nanoclays and promote high tensile strength and optimum mechanical performance. This can be seen at the mechanical performance found at high nanoclay loadings for CMC/MTM = 20/80−40/60. Both samples correspond closely in terms of nanostructure and composition to earlier nacre-mimetics based on LbL or self-assembly of purified core−shell nanoplatelets, and also display similar mechanical properties. Yet, a slight increase of the polymer content in our materials promotes desirable inelastic deformations and frictional sliding of platelets and allows to double and triple the strength values and increase the toughness.

Hence, even if the closest polymer/nanoclay nacre-mimetic would require to have 95 vol % of inorganic material to match the content of the natural role model, the most relevant synthetic bioinspired layered polymer/nanoclay materials might be achieved with less nanoclay, at least at present design levels of the soft phase using commonplace polymers without tailored molecular energy dissipation mechanisms. This is an important factor to consider in the design for future bioinspired materials.

The relevance of these materials as functional coating or barrier foil is emphasized in the high optical transparency as compared for different nanoclay contents in Figure 6b. Lower translucencies for higher nanoclay contents relate to the natural origin of MTM, which contains some contaminants (iron ions) leading to a slightly yellowish color of the nanoclay that translates into the layered nanocomposite. These problems can only be overcome by using synthetic nanoclays, for which there exists however still some limitation in the availability of high-aspect ratio materials required for good mechanical properties. Furthermore, the thermogravimetric analysis reveals an onset of decomposition for the various layered nanocomposites at just below 250 °C. This good thermal stability allows for a substantial application range in engineering materials and functional coatings (Figure 6a).

On the basis of these promising results, we turned to the question whether it would be possible to prepare concentrated slurries of high nanoclay content that are directly suitable for doctor-blading, which is the technologically most relevant coating procedure for thick and infinitely large films. To provide homogeneous dispersions, we used a high-performance kneader with two wide-bladed kneading elements, allowing efficient mixing of tough, nonflowing, highly viscous media. We added solid MTM directly into an agitated 2.5 wt % CMC solution to yield a ca. 3.6 wt % dispersions of CMC/MTM = 60/40 and homogenized it under significant shear of the kneader. Note that we chose one of the optimum compositions, identified in the tensile tests, yet with high content of nanoclay as relevant for functional barrier coatings. We emphasize that such a mixture is impossible to homogenize with a standard magnetic stirrer. Although it seems feasible to prepare higher concentrated gels with kneading, they are not suitable anymore for doctor-blading due to too high gel strength if the concentration is above 4−4.5 wt %. Subsequent doctor-blading of the resulting softer, homogeneous gel allowed thick and translucent self-standing foils, typically prepared in thicknesses from 30−150 μm. Drying at elevated temperature obviously proceeds quicker than when cast from dilute dispersion at comparable film thickness (ca. 50 °C). Further optimization to accelerate the drying in the future is feasible by using CMC of lower molecular weight, which would allow to prepare slurries of higher concentration, yet still at suitable viscosities for doctor-blading. Figure 7a displays a translucent film of roughly a DIN A4 page in size at 50 μm thickness. The microscopic observation of the film shows a preserved highly ordered mesoscale structure of the nanoclay/polymer composite, despite using such a fast macroscopic processing technique (Figure 7b and c). Additional mechanical tensile tests reveal

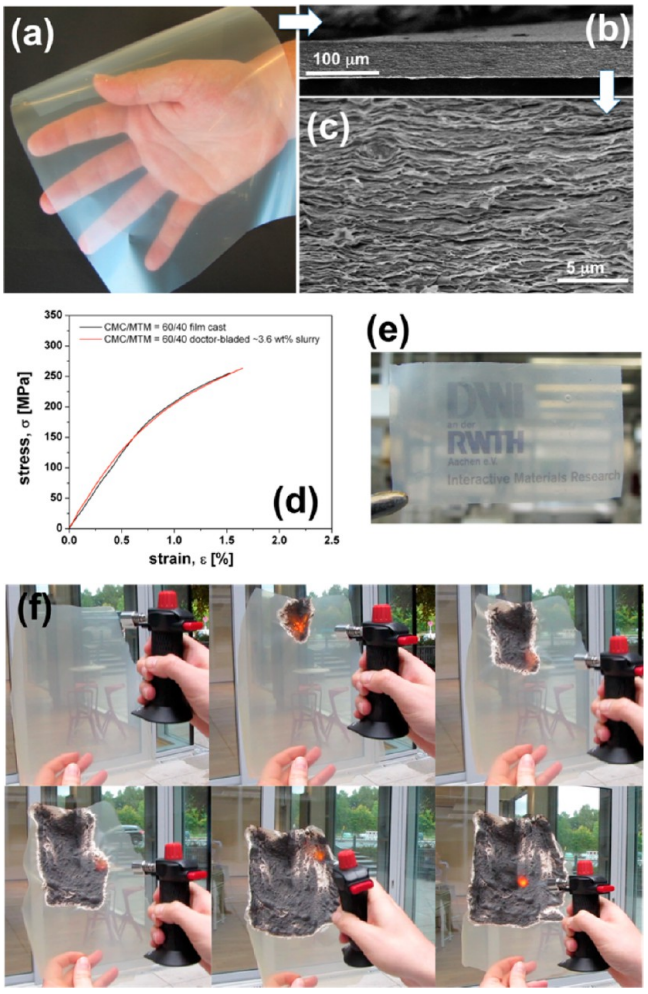

Figure 7. Large-area films prepared by doctor-blading of a CMC/MTM = 60/40 dispersion of high solid content (~3.6 wt %). (a) Nacre-inspired foil being roughly of a DIN A4 page in size and a thickness of 50 μm. (b and c) Overview and higher resolution SEM images, depicting constant film thickness and the layered arrangement of the nanoclays. (d) Comparison of the mechanical tensile properties of the doctor-bladed film and a film cast from dilute dispersions. (e) Institute logo printed on a nacre-inspired bionanocomposite using a commercial deskjet printer. (f) Time-laps series of photographs depicting the fire-blocking properties of the bioinspired films (thickness 120 μm) upon exposure to a butane gas torch (temperature ca. 1300 °C). Note that the material is still translucent and fully self-standing. Flames cannot be observed.

dx.doi.org/10.1021/am400350q | ACS Appl. Mater. Interfaces 2013, 5, 3738−3747

equally good mechanical properties for doctor-bladed films prepared from high concentrations and films cast from dilute dispersions (Figure 7d), thereby validating this direct approach to be applied for continuous roll-to-roll processing.

In terms of functional benefits of these large-scale, nacre-inspired films, we also conducted preliminary experiments on fire-blocking properties and the ability to print on these materials.

The time-laps series of photographs in Figure 7f demonstrates intriguing fire-shielding properties during exposure to the flame of a gas torch. Already at a nanoclay content of only 40% the material hardly burns and is instantly self-extinguishing. Furthermore, it is shape persistent and chars into a solid barrier material resisting longer term exposure to flames. During exposure to flames, the material expands due to gas evolution while burning the intercalated polymer, and a porous foam-like structure develops that provides a heat barrier. Further dehydroxylation of the aluminosilicates contributes to self-cooling via water formation and also mechanical integrity due to char formation.[51,52]

Importantly, the material does not contain halogen atoms or heavy metals, often needed in present-day fire-barrier materials, and can be processed from water using sustainable building blocks. Taking into account that the preparation can be easily scaled to large quantities and coatings and films of high optical quality can be made, we expect that this effort contributes to finding viable, environmentally friendly alternatives for future fire-barrier materials.

Already earlier, we and others demonstrated in a range of studies that such highly loaded and ordered bioinspired nanoclay/polymer composites are excellent gas barrier materials.[17,39,53,54] We will comprehensively address the barrier properties also with respect to oil and water vapor in the future. Herein, we show that large-area self-standing films can be used directly for simple inkjet printing. This is relevant in the context of finding flexible, transparent, oxygen-impermeable substrates for the cost-effective fabrication of printable, oxygen-sensitive, organic electronic devices. The photograph displayed in Figure 7e was obtained using a commercial inkjet printer and inks and demonstrates that already standard inkjet printing settings can be applicable to pattern and structure these nacre-inspired bionanocomposites. Refined and also functional inks and optimized printing procedures can lead to useful devices with enhanced protection against oxygen.

CONCLUSIONS

We demonstrated a facile, large-scale pathway to high-performance, nacre-inspired films with tunable nanoscale periodicity using naturally available building blocks and simple, scalable procedures in water. In terms of applicability it contrasts earlier, more sophisticated, time-consuming preparation strategies for nacre-mimetic materials due to the combination of the simplest and fast preparation with excellent mechanical and functional properties.

The additional advantage to tune the hard/soft ratio and the spacing of the nanoscale periodicity between the nanoclays allowed us to deduce that very high fractions of nanoclay (≥70 wt %), as previously considered optimized in nacre-inspired nanoclay/polymer materials, might in fact not be the ideal composition. Slightly higher polymer contents promote beneficial ductility, inelastic shear deformation, and fracture energy dissipation to allow reaching higher strain-to-failure, toughness, and tensile strength. Overall, this dedicated tuning of the thickness of the soft phase enabled mechanical properties that are among the best ever reported for layered polymer/nanoclay composites and nacre-inspired materials. We foresee that ionic and covalent cross-linking will allow us to further augment the mechanical properties

Concerning a successful water-borne preparation of nacre-inspired films by co-casting at high nanoclay loading from viscous media, the consideration of chemical interactions, correct mixing protocols, and high-shear homogenization are the important parameters to prepare suitable, high-quality, hydrocolloid dispersions for subsequent ordered structure formations. High shear even allows highly homogeneous and concentrated dispersions, suitable to directly prepare films and large-area coatings with essentially the same properties as films cast from dilute dispersions. An extension to higher solid content is feasible by changing to polymers of lower molecular weight, which will be beneficial for transfer to roll-to-roll applications. The developed procedures can be adapted to other systems to access well-ordered films, e.g. synthetic nanoclays for fully transparent materials, or also for (reduced) graphene oxides and other functional nanoplatelets (e.g., BN, MoS_2) which are difficult to prepare as high-quality, concentrated aqueous dispersions.

The excellent mechanical properties and simple preparation are combined with functional benefits—translucency, fire blocking, and ability to pattern the surfaces via inkjet printing—and will help to develop bioinspired materials combining mechanical and functional properties as needed for future applications.

Overall we expect this approach, using naturally occurring components, to promote sustainable alternatives for present-day, high-performance materials combining mechanical and functional properties and push nacre-inspired materials closer to real-life applications.

ASSOCIATED CONTENT

Supporting Information

Additional SEM images of two nanocomposite. This material is available free of charge via the Internet at http://pubs.acs.org.

AUTHOR INFORMATION

Corresponding Author

*E-mail: walther@dwi.rwth-aachen.de.

Notes

The authors declare no competing financial interest.

ACKNOWLEDGMENTS

The authors thank Lars Berglund (KTH, Stockholm) for helpful discussions and Felix Schacher (FSU Jena, Germany) for initial X-ray diffraction measurements. The authors acknowledge financial support from the IGF 17502N grant agreement, the "ERANET Woodwisdom Program", the "Fonds der Chemischen Industrie", and HASYLAB. This work made use of the Aalto University Nanomicroscopy Center (Aalto-NMC) premises. We also thank Franz-Josef Steffens for experimental help. A.W. gratefully acknowledges continuous support by Martin Möller.

REFERENCES

(1) Meyers, M. A.; Chen, P. Y.; Lin, A. Y. M.; Seki, Y. *Prog. Mater. Sci.* **2008**, *53*, 1−206.
(2) Fratzl, P.; Weinkamer, R. *Prog. Mater. Sci.* **2007**, *52*, 1263−1334.
(3) Barthelat, F. *Bioinspiration Biomimetics* **2010**, *5*, 035001.

(4) Wang, J.; Cheng, Q.; Tang, Z. *Chem. Soc. Rev.* **2012**, *41*, 1111−1129.
(5) Corni, I.; Harvey, T. J.; Wharton, J. A.; Stokes, K. R.; Walsh, F. C.; Wood, R. J. K. *Bioinspiration Biomimetics* **2012**, *7*, 031001.
(6) Cartwright, J. H. E.; Checa, A. G. *J. R. Soc., Interface* **2007**, *4*, 491−504.
(7) Podsiadlo, P.; Kaushik, A. K.; Arruda, E. M.; Waas, A. M.; Shim, B. S.; Xu, J.; Nandivada, H.; Pumplin, B. G.; Lahann, J.; Ramamoorthy, A.; Kotov, N. A. *Science* **2007**, *318*, 80−83.
(8) Podsiadlo, P.; Kaushik, A. K.; Shim, B. S.; Agarwal, A.; Tang, Z.; Waas, A. M.; Arruda, E. M.; Kotov, N. A. *J. Phys. Chem. B* **2008**, *112*, 14359−14363.
(9) Podsiadlo, P.; Tang, Z.; Shim, B. S.; Kotov, N. A. *Nano Lett.* **2007**, *7*, 1224−1231.
(10) Bonderer, L. J.; Studart, A. R.; Gauckler, L. J. *Science* **2008**, *319*, 1069−1073.
(11) Bonderer, L. J.; Studart, A. R.; Woltersdorf, J.; Pippel, E.; Gauckler, L. J. *J. Mater. Res.* **2009**, *24*, 2741−2754.
(12) Yao, H. B.; Fang, H. Y.; Tan, Z. H.; Wu, L. H.; Yu, S. H. *Angew. Chem., Int. Ed.* **2010**, *49*, 2140−2145.
(13) Han, J.; Dou, Y.; Yan, D.; Ma, J.; Wei, M.; Evans, D. G.; Duan, X. *Chem. Commun.* **2011**, *47*, 5274−5276.
(14) Munch, E.; Launey, M. E.; Alsem, D. H.; Saiz, E.; Tomsia, A. P.; Ritchie, R. O. *Science* **2008**, *322*, 1516−1520.
(15) Launey, M. E.; Munch, E.; Alsem, D. H.; Barth, H. B.; Saiz, E.; Tomsia, A. P.; Ritchie, R. O. *Acta Mater.* **2009**, *57*, 2919−2932.
(16) Malwitz, M. M.; Dundigalla, A.; Ferreiro, V.; Butler, P. D.; Henk, M. C.; Schmidt, G. *Phys. Chem. Chem. Phys.* **2004**, *6*, 2977−2982.
(17) Ebina, T.; Mizukami, F. *Adv. Mater.* **2007**, *19*, 2450−2453.
(18) Tetsuka, H.; Ebina, T.; Nanjo, H.; Mizukami, F. *J. Mater. Chem.* **2007**, *17*, 3545−3550.
(19) Finnemore, A.; Cunha, P.; Shean, T.; Vignolini, S.; Guldin, S.; Oyen, M.; Steiner, U. *Nat. Commun.* **2012**, *3*, 966.
(20) Lin, T. H.; Huang, W. H.; Jun, I. K.; Jiang, P. *Chem. Mater.* **2009**, *21*, 2039−2044.
(21) Zhou, C. H.; Shen, Z. F.; Liu, L. H.; Liu, S. M. *J. Mater. Chem.* **2011**, *21*, 15132−15153.
(22) Alexandre, M.; Dubois, P. *Mater. Sci. Eng., R* **2000**, *28*, 1−63.
(23) Chiu, C. W.; Lin, J. J. *Prog. Polym. Sci.* **2012**, *37*, 406−444.
(24) Tunc, S.; Duman, O. *Appl. Clay Sci.* **2010**, *48*, 414−424.
(25) Miyamoto, N.; Shintate, M.; Ikeda, S.; Hoshida, Y.; Yamauchi, Y.; Motokawa, R.; Annaka, M. *Chem. Commun.* **2013**, *49*, 1082−1084.
(26) Stefanescu, E. A.; Daly, W. H.; Negulescu, I. I. *Macromol. Mater. Eng.* **2008**, *293*, 651−656.
(27) Pavlidou, S.; Papaspyrides, C. D. *Prog. Polym. Sci.* **2008**, *33*, 1119−1198.
(28) Stefanescu, E. A.; Dundigalla, A.; Ferreiro, V.; Loizou, E.; Porcar, L.; Negulescu, I.; Garno, J.; Schmidt, G. *Phys. Chem. Chem. Phys.* **2006**, *8*, 1739−1746.
(29) Stefanescu, E. A.; Stefanescu, C.; Negulescu, I. I.; Daly, W. H. *Macromol. Chem. Phys.* **2008**, *209*, 2320−2330.
(30) Stefanescu, E. A.; Stefanescu, C.; Donose, B. C.; Garno, J. C.; Daly, W. H.; Schmidt, G.; Negulescu, I. I. *Macromol. Mater. Eng.* **2008**, *293*, 771−780.
(31) Abraham, T. N.; Siengchin, S.; Ratna, D.; Karger-Kocsis, J. *J. Appl. Polym. Sci.* **2010**, *118*, 1297−1305.
(32) Stefanescu, E. A.; Schexnailder, P. J.; Dundigalla, A.; Negulescu, I. I.; Schmidt, G. *Polymer* **2006**, *47*, 7339−7348.
(33) Stefanescu, E. A.; Stefanescu, C.; Daly, W. H.; Schmidt, G.; Negulescu, I. I. *Polymer* **2008**, *49*, 3785−3794.
(34) Dundigalla, A.; Lin-Gibson, S.; Ferreiro, V.; Malwitz, M. M.; Schmidt, G. *Macromol. Rapid Commun.* **2005**, *26*, 143−149.
(35) Shikinaka, K.; Aizawa, K.; Osada, Y.; Shigehara, K. *Chem. Lett.* **2011**, *40*, 1389−1391.
(36) Shikinaka, K.; Aizawa, K.; Fujii, N.; Osada, Y.; Tokita, M.; Watanabe, J.; Shigehara, K. *Langmuir* **2010**, *26*, 12493−12495.
(37) Shikinaka, K.; Aizawa, K.; Murakami, Y.; Osada, Y.; Tokita, M.; Watanabe, J.; Shigehara, K. *J. Colloid Interface Sci.* **2012**, *369*, 470−476.
(38) Zhu, W.; Lu, C. H.; Chang, F. C.; Kuo, S. W. *RSC Adv.* **2012**, *2*, 6295−6305.
(39) Walther, A.; Bjurhager, I.; Malho, J. M.; Pere, J.; Ruokolainen, J.; Berglund, L. A.; Ikkala, O. *Nano Lett.* **2010**, *10*, 2742−2748.
(40) Walther, A.; Bjurhager, I.; Malho, J. M.; Ruokolainen, J.; Berglund, L.; Ikkala, O. *Angew. Chem., Int. Ed.* **2010**, *49*, 6448−6453.
(41) Yao, H. B.; Tan, Z. H.; Fang, H. Y.; Yu, S. H. *Angew. Chem., Int. Ed.* **2010**, *49*, 10127−10131.
(42) Theng, B. K. G. *Clays Clay Miner.* **1982**, *30*, 1−10.
(43) Lee, Y. J.; Kuo, S. W.; Huang, W. J.; Lee, H. Y.; Chang, F. C. *J. Polym. Sci., Part B: Polym. Phys.* **2004**, *42*, 1127−1136.
(44) Kuo, S. W.; Chang, F. C. *Prog. Polym. Sci.* **2011**, *36*, 1649−1696.
(45) Mei, Y.; Lauterbach, K.; Hoffmann, M.; Borisov, O. V.; Ballauff, M.; Jusufi, A. *Phys. Rev. Lett.* **2006**, *97*, 158301.
(46) Henle, M. L.; Santangelo, C. D.; Patel, D. M.; Pincus, P. A. *Europhys. Lett.* **2004**, *66*, 284−290.
(47) Manning, G. S. *J. Chem. Phys.* **1969**, *51*, 924−933.
(48) Plamper, F. A.; Walther, A.; Müller, A. H. E.; Ballauff, M. *Nano Lett.* **2007**, *7*, 167−171.
(49) Ashby, M. F.; Gibson, L. J.; Wegst, U.; Olive, R. *Proc. R. Soc. London, Ser. A* **1995**, *450*, 123−140.
(50) Tetsuka, H.; Ebina, T.; Tsunoda, T.; Nanjo, H.; Mizukami, F. *Jpn. J. Appl. Phys.* **2008**, *47*, 1894−1896.
(51) Kiliaris, P.; Papaspyridis, C. D. *Prog. Polym. Sci.* **2010**, *35*, 902−958.
(52) Davis, R. D.; Gilman, J. W.; VanderHart, D. L. *Polym. Degrad. Stab.* **2003**, *79*, 111−121.
(53) Priolo, M. A.; Gamboa, D.; Holder, K. M.; Grunlan, J. C. *Nano Lett.* **2010**, *10*, 4970−4974.
(54) Choi, J. H.; Park, Y. W.; Park, T. H.; Song, E. H.; Lee, H. J.; Kim, H.; Shin, S. J.; Lau, V. C. F.; Ju, B. K. *Langmuir* **2012**, *28*, 6826−6831.